Scheme IV

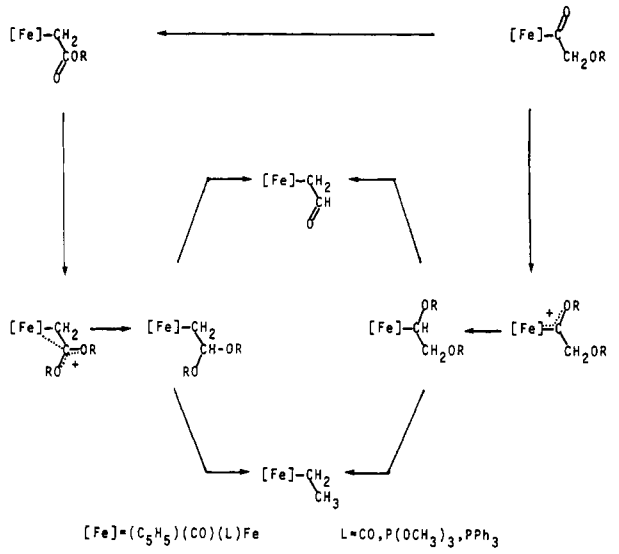

it is quite reasonable that an alkoxyborane could abstract β-alkoxide with or without hydride transfer and give (perhaps competitively) the mixture of **15** and **16**, respectively.

Release of acetaldehyde with acid from the formylmethyl complex **19** was demonstrated although as already noted the analytical chemistry was both tedious and of limited accuracy. Nevertheless, significant amounts of acetaldehyde did form. A plausible mechanism for this release of acetaldehyde, which will be documented for our results with the analogous Fp system,[15] entails protonolysis of **19** by electrophilic attack on iron rather than by dissociation of vinyl alcohol from **21** (eq 13). (The

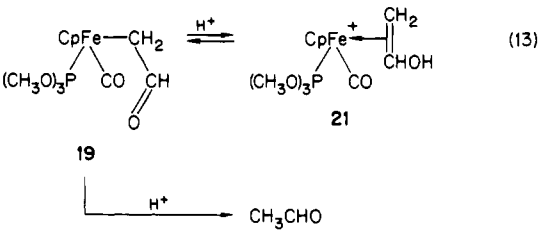

(13)

corresponding η^2-vinyl ether complex **18** does not dissociate vinyl ether under comparable—or more extreme—reaction conditions.]

In summary, the carbalkoxymethyl ligand serves as a viable C_2 template in selectively generating other C_2 ligands and organic molecules. Certainly with the aforementioned availability and reactivity of the carbalkoxymethyl ligand, it would prove interesting to generate these systems using more labile organometallic complexes—particularly those that might add H_2 and reductively eliminate acetic acid esters. In terms of procuring acetaldehyde, Scheme IV outlines our "β-activation" route in generating a formylmethyl complex from the carbalkoxymethyl system. It is also worth noting that these results complement those that define the α-activation coordinated ligand route for transforming a C_2 alkoxyacetyl ligand into the same formylmethyl and ethyl groups. Progress of studies using either (1) more labile metal complexes and H_2 or (2) organometallic Lewis acids and hydrido complexes in place of the carbocationic activating groups and borohydride reagents to selectively (but stoichiometrically) generate C_2 and C_3 ligands and organic products will be reported in due course.

Acknowledgment. Support from the Department of Energy, Office of Basic Energy Sciences, is gratefully acknowledged.

(49) Vinyl alcohol or vinyl ether complexes with a more sterically hindered metal center, such as Co(III) in cobaloxime η^2-vinyl ether compounds can directly dissociate the vinyl ether and possibly vinyl alcohol (acetaldehyde) in analogous reactions. Silverman, R. B.; Dolphin, D. *J. Am. Chem. Soc.* **1976**, *98*, 4633.

Structure of Rhodium in an Ultradispersed Rh/Al_2O_3 Catalyst as Studied by EXAFS and Other Techniques

H. F. J. van 't Blik,† J. B. A. D. van Zon, T. Huizinga,‡ J. C. Vis, D. C. Koningsberger, and R. Prins*

Contribution from the Laboratory for Inorganic Chemistry, Eindhoven University of Technology, 5600 MB Eindhoven, The Netherlands. *Received June 25, 1984*

Abstract: The structure of rhodium in an ultradispersed 0.57 wt % Rh/γ-Al_2O_3 catalyst before and after CO adsorption was studied with extended X-ray absorption fine structure (EXAFS), X-ray photoelectron spectroscopy (XPS), electron spin resonance (ESR), temperature programmed reduction (TPR), CO infrared spectroscopy, and H_2 and CO chemisorption. With the aid of these complementary techniques, it could be established that the structure of the rhodium catalyst was completely different before and after CO adsorption. Before CO adsorption and after reduction of the catalyst at 593 K, all the rhodium was reduced and in the form of three-dimensional metallic crystallites. CO adsorption disrupted the metal–metal bonds in the crystallites, leading to isolated rhodium geminal dicarbonyl species in which the rhodium was present as Rh^+. Each rhodium ion was surrounded by two carbon monoxide molecules and three oxygen anions of the support.

As a result of many industrial applications, such as the hydrogenation of carbon monoxide, the reduction of nitrogen monoxide in automobile exhaust gas, and the hydroformylation of olefins, catalysts consisting of finely dispersed rhodium supported on alumina are studied extensively. The use of very well dispersed rhodium on a support is not only of obvious importance from an economical point of view but also from the point of view of activity and selectivity of the catalysts. Thus Yao et al.[1] reported that in going from a well dispersed rhodium phase to a particulate phase the specific activity for *n*-pentane hydrogenolysis decreased and the activity for reduction of NO by hydrogen increased. Alterations in the reaction parameters and in the product dis-

† Present address: Philips Research Laboratories, P.O. Box 80.000, 5600 JA Eindhoven, The Netherlands.

‡ Present address: Koninklijke/Shell-Laboratorium, Badhuisweg 3, 1031 CM Amsterdam, The Netherlands.

(1) Yao, H. C.; Yu Yao, Y. F.; Otto, K. *J. Catal.* **1979**, *56*, 21.

0002-7863/85/1507-3139$01.50/0

tributions indicated strongly that the reaction intermediate in the *n*-pentane hydrogenolysis and the rate-determining step in the NO reduction changed if the rhodium surface phase changed.

Although many detailed characterization studies of highly dispersed rhodium catalysts have been reported, the state of the metal is not yet known exactly. There even exists a controversy about the structure and oxidation state of the rhodium in these systems after reduction with hydrogen. Infrared spectroscopy has been used as a sensitive tool to study the variations in carbon–oxygen stretching frequencies of CO chemisorbed on Rh/Al_2O_3 catalysts.[2-10] These variations are due to subtle changes in the character of the supported rhodium. For highly dispersed rhodium catalysts two CO bands are observed around 2095 and 2027 cm^{-1}, representing the symmetrical and antisymmetrical stretching modes of the CO molecules bound to one surface rhodium atom. The wavenumbers of this so-called geminal dicarbonyl rhodium species correspond closely to those observed for the bridged $\{Rh(CO)_2Cl\}_2$ complex and do not shift in frequency with increasing CO coverage. On the basis of these data some investigators have asserted that rhodium on Al_2O_3 is monatomically dispersed and is in the Rh^+ state.[2-6]

However, Primet has shown that for rhodium supported on alumina the geminal dicarbonyl species are not formed at low temperature but develop on warming to room temperature.[7] He assumed that after reduction of the catalyst the rhodium is fully reduced and that upon CO admission CO dissociates at room temperature and excess CO adsorbs on the resulting surface Rh–O species, giving the dicarbonyl species. There are also other strong indications that rhodium is present as metallic crystallites after reduction with hydrogen. Detailed studies have been performed on these dispersed systems by using catalytic reactions[1,11] (e.g., hydrogenolysis, which is catalyzed by metals only) as well as chemisorption and electron microscopy.[8,9] From the electron microscopy studies one has concluded that rhodium is present in two-dimensional rafts.[8,9] In these studies also CO infrared measurements were carried out and the observed $Rh(CO)_2$ species was assigned to two CO molecules adsorbed on the edge atoms of these two-dimensional rafts.

In order to obtain more insight into the structure of rhodium and the influence of CO adsorption on this structure we have studied a reduced highly dispersed 0.57 wt % Rh/γ-Al_2O_3 catalyst before and after CO admission by a number of complementary techniques. The results of this study are presented in this paper; some preliminary results have been published before.[10] It will be shown that the results of our study allow us to resolve the seeming contradiction between the results obtained by infrared studies and those obtained by high resolution electron microscopy studies: Rh–Rh metallic bonds are observed in a fully reduced Rh/Al_2O_3 catalyst, while these bands are broken upon CO adsorption.

The techniques used in the present study are extended X-ray absorption fine structure spectroscopy (EXAFS), X-ray photoelectron spectroscopy (XPS), electron spin resonance (ESR), temperature programmed reduction (TPR), CO infrared spectroscopy, and H_2 and CO chemisorption. As the detailed analysis of the EXAFS of the Rh K-edge of the reduced system is being published separately,[12] only the quantitative results of the reduced system will be presented in this paper. However, an extensive description of the EXAFS analysis of the catalyst after CO adsorption will be given. For the sake of clearness we have, therefore, divided the sections Results and Discussion into two parts. The first part deals with the structure of the reduced system, and in that part it will be shown that after reduction of the impregnated rhodium catalyst only metallic rhodium particles are present. The second part deals with the structure of the catalyst system after CO adsorption. There evidence will be given that the small metallic particles are converted to isolated geminal dicarbonyl species upon CO adsorption at room temperature.

Experimental Section

Catalyst Preparation. A 0.57 wt % Rh/γ-Al_2O_3 catalyst was prepared by incipient wetting of γ-Al_2O_3 with an aqueous solution of $RhCl_3 \cdot xH_2O$ (Drijfhout & Zn.). The support γ-Al_2O_3 (BET area of 150 $m^2\ g^{-1}$ and a pore volume of 0.65 $cm^3\ g^{-1}$) was obtained by heating boehmite (Martinswerk, GmbH) at 873 K. After impregnation the catalyst was dried in air at 393 K for 20 h to remove the adsorbed water and stored for further use. The rhodium content was determined colourimetrically. A 2 wt % Rh/γ-Al_2O_3 catalyst was prepared by using the dimer $\{Rh(CO)_2Cl\}_2$ as precursor. The dimer was prepared from $RhCl_3 \cdot xH_2O$ and CO as described by McCleverty and Wilkinson.[13] In this case the support used was a Ketjen γ-Al_2O_3 (000–1.5E, S.A. = 200 $m^2\ g^{-1}$, pore volume = 0.60 $cm^3\ g^{-1}$). The support was dispersed in *n*-hexane to which a solution of $\{Rh(CO)_2Cl\}_2$ in *n*-hexane was added. After 2 h this mixture had decolorized, which indicated that the exchange was complete. After being filtered the catalyst was vacuum dried at 298 K for 30 min and stored.

Chemisorption. Chemisorption measurements were performed in a conventional glass system at 298 K. Research grade CO was used without further purification. Hydrogen was purified by passing it through a Pd diffusion cell. Before the measurement of the CO and H_2 chemisorption the dried catalyst was reduced at 593 K (heating rate of 5 deg K/min) for 1 h under flowing hydrogen and then evacuated (10^{-2} Pa) at 573 K for 1 h. The measurement was carried out as follows: After reduction and evacuation of the catalyst approximately 70 kPa of H_2 or CO was admitted. When equilibrium was reached the pressure in the system was diminished in steps of about 10 kPa by pumping away a known amount of gas. As we measured from high to low pressure we will use the term desorption isotherm instead of adsorption isotherm. Following the method of Benson and Boudart[14] one obtains the total amount of chemisorbed H atoms and CO molecules by extrapolating the linear higher pressure region ($P > 30$ kPa, where monolayer coverage is reached) of the isotherm to zero pressure and by correcting for the extrapolated value of the bare support.

TPR. The thermoreduction studies were performed in an apparatus similar to the one which has extensively been described by Boer et al.[15] A mixture of 5% H_2 in Ar was used for the reduction. This mixture was purified over molecular sieves for the removal of water and over a BTS column for the removal of traces of oxygen. By using a thermal conductivity detector (TCD) of the diffusion type the difference between the hydrogen concentration of the mixture entering and leaving the reactor can be detected. The TCD signal monitored as a function of temperature yields the TPR profile. The heating rate during all TPR measurements was 5 deg K/min, and the gas flow rate was 300 Nl/h. Since water is formed during reduction of the supported oxides by hydrogen, the gas coming from the reactor is dried over magnesium perchlorate before entering the thermal conductivity cell. Before the reduction was performed the catalyst was dried in argon at 393 K for 1 h in the reactor of the TPR apparatus and was subsequently cooled to 223 K (a supply of liquid coolant is present). The amount of consumed gas during TPR is expressed per total amount of metal, H_2/Rh. As the oxidation state of rhodium in the impregnated and oxidized catalyst is 3+, the theoretical H_2/Rh value is 1.5. The accuracy of the H_2/Rh values is ±5%.

ESR. To measure ESR spectra in situ we used a reactor designed by Konings et al.[16] X-band ESR spectra were recorded with a Varian E-15 spectrometer equipped with a TE-104 dual sample cavity. Signal intensity, position of the signal, and quality factor of the ESR cavity were calibrated with the aid of a Varian strong pitch sample (g = 2.0028, 3 × 10^{15} spins/cm). The ESR spectra were recorded at 20 K.

(2) Yang, A. C.; Garland, C. W. *J. Phys. Chem.* **1957**, *61*, 1504.
(3) Rice, C. A.; Worley, S. D.; Curtis, C. W.; Guin, J. A.; Tarrer, A. R. *J. Chem. Phys.* **1981**, *74*, 6487.
(4) Cavanagh, R. R.; Yates, J. T. *J. Chem. Phys.* **1981**, *74*, 4150.
(5) Worley, S. D.; Rice, C. A.; Mattson, G. A.; Curtis, C. W.; Guin, J. A.; Tarrer, A. R. *J. Phys. Chem.* **1982**, *86*, 2714.
(6) Worley, S. D.; Rice, C. A.; Mattson, G. A.; Curtis, C. W.; Guin, J. A.; Tarrer, A. R. *J. Chem. Phys.* **1982**, *76*, 20.
(7) Primet, M. *J. Chem. Soc., Faraday Trans. 1* **1978**, *74*, 2570.
(8) Yates, D. J. C.; Murrell, L. L.; Prestridge, E. B. *J. Catal.* **1979**, *57*, 41.
(9) Yates, D. J. C.; Murrell, L. L.; Prestridge, E. B. "Growth and Properties of Metal Clusters"; Bourdon, J. Ed.; Elsevier Scientific Publishing Co.: Amsterdam, 1980; p 137.
(10) van 't Blik, H. F. J.; Van Zon, J. B. A. D.; Huizinga, T.; Vis, J. C.; Koningsberger, D. C.; Prins, R. *J. Phys. Chem.* **1983**, *87*, 2264.
(11) Graydon, F. W.; Langan, M. D. *J. Catal.* **1981**, *69*, 180.
(12) Van Zon, J. B. A. D.; Koningsberger, D. C.; van 't Blik, H. F. J.; Sayers, D. E. *J. Chem. Phys.*, to be published.
(13) McCleverty, J. A.; Wilkinson, G. *Inorg. Synth.* **1966**, *8*, 211.
(14) Benson, J. E.; Boudart, M. *J. Catal.* **1965**, *4*, 704.
(15) Boer, H.; Boersma, W. J.; Wagstaff, N. *Rev. Sci. Instrum.* **1982**, *53*, 349.
(16) Konings, A. J. A.; Van Dooren, A. M.; Koningsberger, D. C.; De Beer, V. H. J.; Farragher, A. L.; Schuit, G. C. A. *J. Catal.* **1978**, *54*, 1.

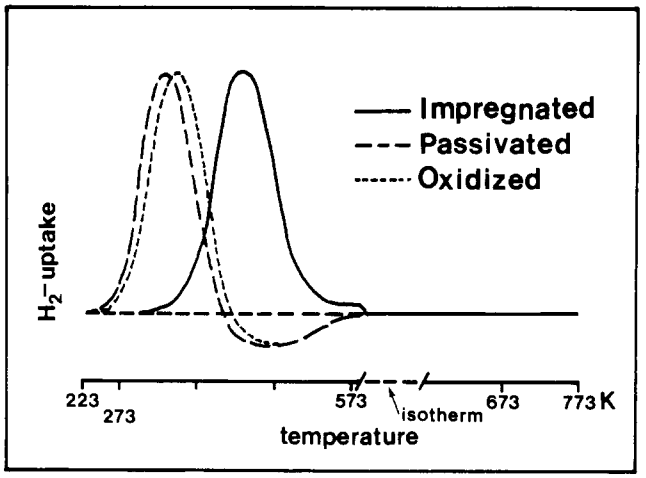

Figure 1. TPR of 0.57 wt % Rh/γ-Al_2O_3 after impregnation, reduction at 773 K and passivation, and reduction at 773 K and oxidation at 773 K.

XPS. XPS measurements were carried out on a Physical Electronics 550 XPS/AES spectrometer equipped with a magnesium anode ($h\nu$ = 1253.6 eV) and a double pass cylindrical mirror analyzer. Prior to the measurements, the passivated powdered sample was pressed on a stainless steel grid, which was mounted onto a heatable transfer rod.[17] The catalysts were prepared on the rod in a preparation chamber attached to the UHV work chamber. After the treatment the preparation chamber was evacuated to 6.6×10^{-3} Pa at 298 K after which the rod was transported via a gate valve to the work chamber and positioned in front of the analyzer and X-ray source. The pressure during the measurements did not exceed 6.6×10^{-6} Pa, and the temperature was approximately 313 K. The binding energies, referenced to the Fermi level, were calibrated by adjusting the C 1s energy at 284.6 eV. The Al 2p (74.4 eV) binding energy of the support was used as a check on the carbon reference. The accuracy of the binding energies is 0.1 eV.

IR Spectroscopy. Infrared spectra were recorded at 298 K with a Bruker IFS 113v Fourier transform spectrometer with a resolution of 2 cm^{-1}. After prereduction at 593 K and passivation at room temperature, the catalyst was pressed in a thin self-supporting wafer and placed in an infrared cell suitable for in situ measurements.[18] In the cell the catalyst was reduced at 523 K and evacuated and then cooled to room temperature. After CO admission (50 kPa) the catalyst was pumped off again before measuring the infrared spectrum.

EXAFS. The EXAFS experiments were performed on X-ray beam line I-5 at the Stanford Synchrotron Radiation Laboratory (SSRL) with a ring energy of 3 GeV and a ring current between 40 and 80 mA. The EXAFS spectra were recorded at liquid nitrogen temperature in an in situ cell.[19] The samples were pressed into a thin self-supporting wafer and mounted in the sample cell. The reduction procedure of the 0.57 wt % Rh/γ-Al_2O_3 catalyst was identical with the one preceding the chemisorption measurements. After in situ EXAFS experiments of the reduced catalyst (under 100 kPa of H_2) the cell was evacuated at 573 K for 1 h. After being cooled in vacuum (10^{-2} Pa) to room temperature the sample was exposed to 100 kPa of CO and the EXAFS spectrum was again recorded in situ.

With a data analysis procedure described by van Zon et al.[12], the EXAFS data were analyzed by using phase and amplitude functions obtained from reference samples with known crystallographic structure. Rh foil, powdered Rh_2O_3, powdered $RhCl_3$, and $\{Rh(CO)_2Cl\}_2$ were taken as reference compounds. The powders and the dimer were mixed with respectively alumina and silica in order to obtain an optimal absorption with respect to the signal-to-noise ratio.

Results

The Structure of Rhodium after Reduction. TPR. In Figure 1 the TPR profile of the impregnated and dried Rh/γ-Al_2O_3 catalyst is given. The reduction was performed in two steps. First the temperature was increased up to 593 K and held at that temperature for 1 h (the normal reduction procedure of the catalyst before each measurement), followed by a further reduction up to 773 K. It is important to note that after reduction at 593 K no more hydrogen was consumed, which indicates that the reduction was complete. Also the H_2/Rh value of 1.43 (Table I) shows that the majority of Rh^{3+} had been reduced, since the reduction degree is $1.43/1.50 = 0.95 \pm 0.05$. These results are in accordance with those reported by Newkirk and McKee.[20] By using thermogravimetric analysis they found that reduction temperatures in the range of 423–473 K are sufficient to reduce rhodium chloride to the elemental metal. Although one cannot dismiss the possibility that the degree of reduction of the passivated catalyst is a little less than 100% one can exclude the possibility that after reduction much rhodium is present as isolated Rh^{n+} ions. If the oxidation state of rhodium would have been 1+, the maximum H_2/Rh value should have been 1.00, which is much lower than the value of 1.43 found experimentally. In Figure 1 also the TPR profiles are presented for a passivated (oxidation at 298 K) Rh/γ-Al_2O_3 catalyst and a catalyst oxidized at 773 K, which had been prereduced at 773 K for 1 h. The corresponding H_2/Rh values are given in Table I. For the passivated catalyst an H_2/Rh value of 1.36 was observed, which shows that passivation leads to a high degree of oxidation for highly dispersed rhodium supported on γ-Al_2O_3. If the oxidation would have been complete, an H_2/Rh value of 1.5 would have been found, according to the following reaction: $Rh_2O_3 + 1.5H_2 \rightarrow 2Rh + 3H_2O$. The TPR profile observed for the catalyst which had been preoxidized at 773 K is characterized by a single peak at 358 K. The total H_2/Rh value of 1.41 indicates that rhodium was mainly present as Rh_2O_3. The peak maximum of the profile shifted from 343 to 358 K when the oxidation temperature was increased from 298 to 773 K. During passivation a more open structure of the rhodium oxide, probably with more defects, may be formed than after oxidation of the catalyst at high temperature. Since nucleation is a very important step in the reduction of the oxide and since reduction starts more easily at a defect, it can be understood that the passivated catalyst reduces at a somewhat lower temperature. Yao et al.[21,22] found for Rh/Al_2O_3 samples, which were reduced at 973 K and subsequently oxidized at 773 K, a reduction peak at 373 K, while in our case the peak maximum is at 358 K. However, they used a heating rate of 8 deg K/min whereas we used 5 deg K/min. It is known that higher heating rates shift the peaks to higher temperatures.[23]

Table I. Hydrogen Consumption during Temperature-Programmed Reduction of 0.57 wt % Rh/γ-Al_2O_3 after Different Treatments

treatment	H_2/Rh
impregnation	1.43
reduction at 773 K, passivation	1.36
reduction at 773 K, oxidation at 773 K	1.41

Hydrogen Chemisorption. The measurement resulted in an H/Rh ratio of 1.7, indicating a highly dispersed metallic system. H/Rh values higher than 1 on Rh/Al_2O_3 catalysts have been observed before[21,24] and are explained by multiple adsorption, although hydrogen spillover cannot be excluded.[25]

ESR. After reduction of the catalyst at 593 K and evacuation at 298 K, to avoid condensation at low temperature, an ESR signal was observed with $g = 2.14$ and $\Delta H = 260$ G (Figure 2a). From the signal intensity it is calculated that 4.8% of the rhodium atoms are paramagnetic with $S = {}^1/_2$. Within the experimental error this is in accordance with the reduction degree of 95% as observed by TPR. The ESR signal is attributed to Rh^{2+} (d^7) ions and not to Rh^0 (d^8s^1) atoms, because the signal did not change in intensity when the reduction at 293 K was prolonged for a long time. As

(17) Huizinga, T.; van 't Blik, H. F. J.; Vis, J. C.; Prins, R. *Surf. Sci.* **1983**, *135*, 580.
(18) Vis, J. C. Thesis, University of Technology Eindhoven, 1984.
(19) Koningsberger, D. C.; Cook, J. W. "EXAFS and Near Edge Structures"; Bianconi, A., Incoccia, L., Stipcich, S., Eds.; Springer-Verlag: Berlin, 1983; p 412.
(20) Newkirk, A. E.; McKee, D. W. *J. Catal.* **1968**, *11*, 370.
(21) Yao, H. C.; Japar, S.; Shelef, M. *J. Catal.* **1977**, *50*, 407.
(22) Yao, H. C.; Shelef, M. "Proceedings of the 7th International Congress on Catalysis"; Weiyama, T., Tanabe, T. Eds.; Elsevier: Amsterdam, 1981; Part B, p 329.
(23) Hurst, N. W.; Gentry, S. J.; Jones, A. *Catal. Rev.-Sci. Eng.* **1982**, *24*, 233.
(24) Wanke, S. E.; Dougharty, N. A. *J. Catal.* **1972**, *24*, 367.
(25) Cavanagh, R. R.; Yates, J. T., Jr. *J. Catal.* **1981**, *68*, 22.

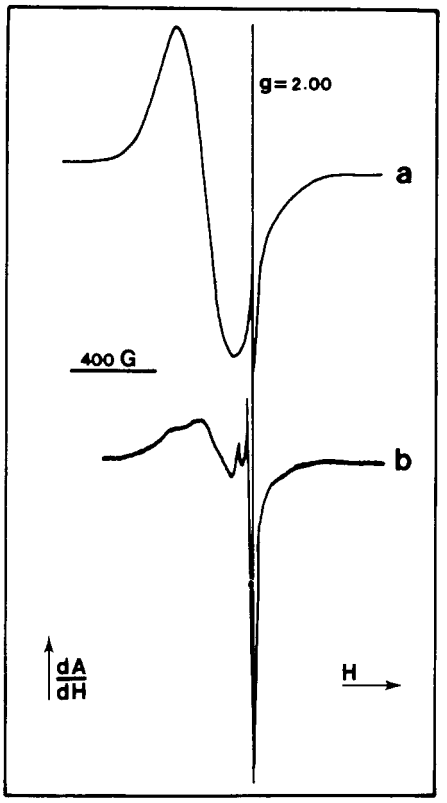

Figure 2. X-band ESR spectra of 0.57 wt % $Rh/\gamma\text{-}Al_2O_3$ recorded at 20 K after (a) reduction at 593 K and evacuation at 298 K and (b) reduction and evacuation at 593 K and CO admission and evacuation at 298 K.

Table II. X-ray Photoelectron Spectroscopy

	binding energy of Rh $3d_{5/2}$ (eV)
0.57 wt % $Rh/\gamma\text{-}Al_2O_3$	
impregnation	310.7
reduction at 593 K	307.5
Rh foil	307.0
0.57 wt % $Rh/\gamma\text{-}Al_2O_3$	
reduction at 593 K, evacuation at 593 K, CO admission at 298 K	308.7
ion exchanged $\{Rh^+(CO)_2Cl\}_2/\gamma\text{-}Al_2O_3$	308.6
$\{Rh^+(CO)_2Cl\}_2$	308.8

the mobility of rhodium atoms is substantial, one would expect sintering of isolated Rh^0 atoms and consequently a decrease of the ESR signal with reduction time. Since this did not occur we assign the ESR signal to Rh^{2+} ions and exclude the possibility that isolated Rh^0 atoms are present after reduction of the catalyst.

Thus from the TPR, chemisorption, and ESR results it can be concluded that in the highly dispersed 0.57 wt % $Rh/\gamma\text{-}Al_2O_3$ catalyst the major part of the rhodium is present in the form of metal crystallites.

XPS. We used XPS as a complementary technique in order to support the TPR and ESR observation that the oxidation state of rhodium after reduction of the catalyst is zero. In Table II the rhodium $3d_{5/2}$ electron binding energies of the impregnated and the reduced catalyst are presented. (In all samples the $3d_{3/2}$–$3d_{5/2}$ doublet separation is the same, 4.5 eV). Although the TPR results demonstrate that after reduction the catalyst has been reduced completely, the rhodium $3d_{5/2}$ electron binding energy of the reduced catalyst (307.5 eV) is somewhat higher than the Rh $3d_{5/2}$ value of the foil (307.0 eV). This observation, previously reported by Huizinga et al.,[17] is explained by the so-called final state effect. Because of screening of the created core-hole by the electrons of neighboring atoms, the apparent binding energy is lowered. This lowering is maximum for bulk

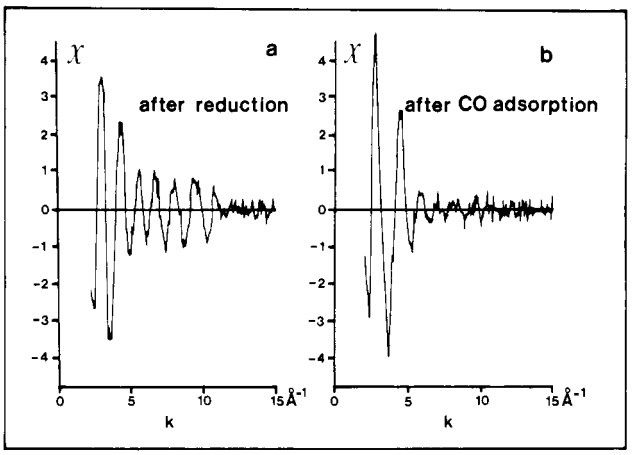

Figure 3. The primary EXAFS data of the rhodium K-edge at 77 K of the 0.57 wt % $Rh/\gamma\text{-}Al_2O_3$ catalyst after (a) reduction at 593 K (100 kPa of H_2) and (b) CO adsorption at room temperature (100 kPa of CO).

atoms, because they have more neighboring atoms and thus more screening electrons. In the reduced catalyst the metal particles are very small and consequently an Rh atom will on the average have less neighboring atoms and as a consequence the core-hole screening will be less effective. This leads to an apparent binding energy which is higher than that of bulk Rh.[26] In agreement with this explanation it was shown in a previous study[17] that sintering leads to a decrease of the binding energy.

From the intensities of the various lines and using Scofield's cross sections[27] we calculated an atomic Cl/Rh ratio of 4.8 and 4.0 for respectively the impregnated catalyst and the catalyst reduced at 593 K for 1 h. Although these values are not very accurate, we can at least conclude that after reduction the majority of the chloride is still present on the surface of the support.

EXAFS. In order to obtain more insight into the structure of the metallic crystallites, EXAFS measurements were performed on the catalyst which was reduced at 593 K for 1 h. The EXAFS of the rhodium K-edge of the reduced catalyst is presented in Figure 3a.

As described in a previous paper, the EXAFS oscillations of the rhodium K-edge of a reduced highly dispersed Rh/Al_2O_3 catalyst are a sum of oscillations due to metallic rhodium and support oxygen scatterers.[28] To obtain this information a modification of the usual data analysis procedures has been applied.[12] Only a brief description of this analysis will be given here.

In general, the Fourier transform (FT) of an Rh–Rh EXAFS function consists of a main peak and a side lobe at lower r values, which is typical for high-Z elements. The origin of this is the nonlinear k dependence of the back-scattering amplitude as well as the phase-shift function. This means that the side lobe in the FT of reduced Rh/Al_2O_3 may interfere in the r region, where distances due to support oxygen are to be expected. By correcting the FT for the rhodium phase shift and backscattering amplitude the Rh–Rh contribution will appear as a single localized peak without side lobes. The contributions of the support oxygen to the FT of the EXAFS function can now more easily be identified. From the FT of the catalyst reliable parameters for the rhodium and rhodium-support oxygen can be determined. The optimized parameters associated with the catalyst are summarized in Table III.

The Structure of Rhodium after CO Admission. CO Chemisorption. A CO/Rh ratio of 1.9 was observed after correction for adsorption onto the bare support, which was substantially more (43 μmol of CO per g of catalyst) than for hydrogen (1 μmol of H_2 per g of catalyst). The CO/Rh value of 1.9 points to the formation of rhodium geminal dicarbonyl species and furthermore

(26) Wertheim, G. K.; Cenzo, D.; Youngquist, S. E. *Phys. Rev. Lett.* **1983**, *51*, 2310.
(27) Scofield, J. H. *J. Electron Spectrosc. Relat. Phenom.* **1976**, *8*, 129.
(28) van Zon, J. B. A. D.; Koningsberger, D. C.; Sayers, D. E.; van 't Blik, H. F. J.; Prins, R. *J. Chem. Phys.* **1984**, *80*, 3914.

Table III. EXAFS Parameter Values for the 0.57 wt % Rh/γ-Al_2O_3 Catalyst after Reduction and CO Admission[a]

	coordination								
	Rh–Rh			Rh–O			Rh–CO		
treatment	N	R (Å)	$\Delta\sigma^2 \times 10^2$ (Å^2)	N	R (Å)	$\Delta\sigma^2 \times 10^2$ (Å^2)	N	R (Å)	$\Delta\sigma^2 \times 10^2$ (Å^2)
reduction at 593 K	3.7	2.68	0.5	1.9	2.74	0.0			
reduction at 593 K, evacuation at 593 K, CO admission at 298 K				3.1	2.12	0.3	1.8		0.7

[a] Accuracies: N, ±15%; R, ±1%; $\Delta\sigma^2$, ±15%.

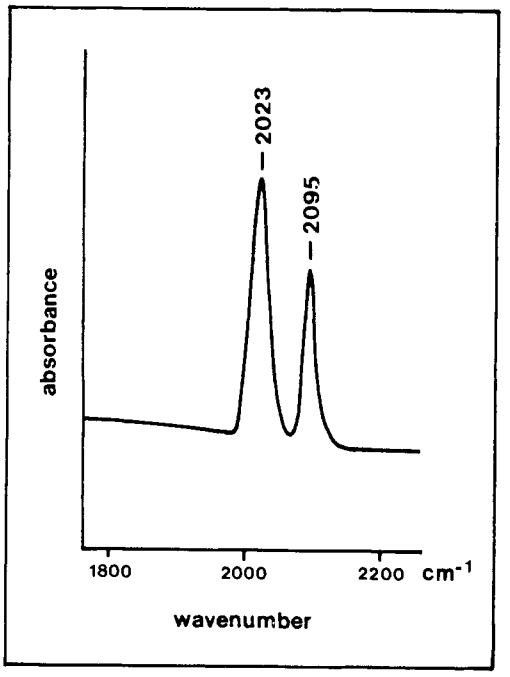

Figure 4. CO infrared spectrum on a 0.57 wt % Rh/γ-Al_2O_3 catalyst (measured at 298 K).

indicates that the catalyst is ultradispersed.

Infrared. Figure 4 shows the 1800–2200 cm^{-1} region of the infrared spectrum of the reduced and evacuated catalyst. After exposure to CO (50 kPa) and evacuation at 298 K only two infrared bands at 2095 and 2023 cm^{-1} are present, which are assigned to the symmetrical and antisymmetrical stretching frequencies of the $Rh(CO)_2$ species. This result is in accordance with the results of Cavanagh and Yates[4] on a 0.2 wt % Rh/Al_2O_3 catalyst and of Rice and Worley et al.[3] and Yates et al.[8,9] on a 0.5 and a 1.0 wt % Rh/Al_2O_3 catalyst.

EXAFS. In Figure 3b the oscillatory EXAFS function $\chi(k)$ of the rhodium K-edge of the catalyst is shown after CO adsorption at room temperature. The most striking feature is the significant decrease of the oscillations above k = 5 Å^{-1}, which are typical for the Rh–Rh metal coordination, compared to the EXAFS oscillations of the reduced catalyst (see Figure 3a). This result was already reported in a previous publication.[10] It clearly shows the dramatic influence of CO adsorption on the highly dispersed Rh/Al_2O_3 catalyst. A disruption of rhodium–rhodium metallic bonds takes place as a result of the chemisorption of CO molecules. As proven by infrared, only $Rh(CO)_2$ species exist after CO admission. An answer to the intriguing question regarding the binding mechanism between the $Rh(CO)_2$ species and the support will be obtained by a careful analysis of the EXAFS data presented in Figure 3b. In order to interpret the EXAFS spectrum of the catalyst after CO admission, it is necessary to use a suitable reference compound for the rhodium geminal dicarbonyl ($Rh(CO)_2$) species which are formed on the catalyst surface. For this purpose we used the dimer $\{Rh(CO)_2Cl\}_2$ since it has the same CO infrared bands as the catalyst after CO admission. The crystalline structure of the dimer is presented in Figure 5.[29] A minor advantage for taking the dimer as a reference compound is its good stability in an oxygen atmosphere, thus facilitating the EXAFS measurement.

(29) Dahl, L. F.; Martell, C.; Wampler, D. L. *J. Am. Chem. Soc.* **1961**, *83*, 1761.

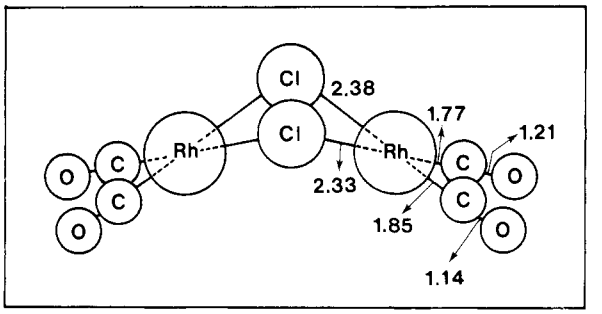

Figure 5. Bond lengths (Å) in $\{Rh(CO)_2Cl\}_2$.

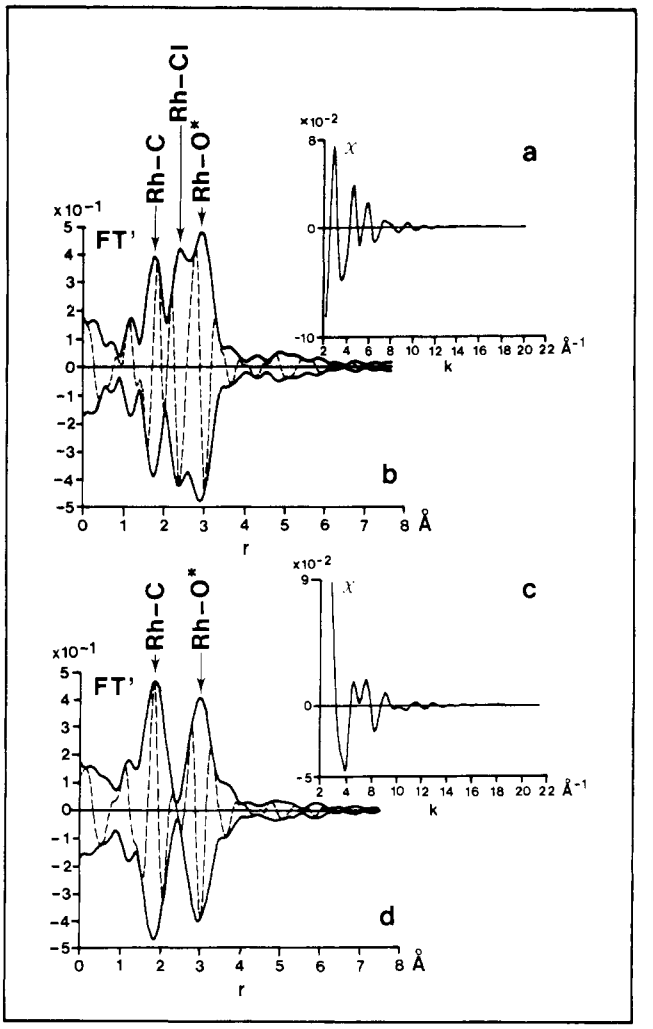

Figure 6. The dimer $\{Rh(CO)_2Cl\}_2$: (a) the normalized primary EXAFS data of the rhodium K-edge at 77 K; (b) the associated k^2-weighed Fourier transform (Δk = 2.44–12.6 Å^{-1}, Rh–O phase shift corrected) [solid line = |FT'|, dotted line = ImFT']; (c) the difference between the normalized EXAFS data and the calculated contribution of the nearest neighbor chlorine atoms; (d) the k^2-weighed Fourier transform of the difference signal (Δk = 3.3–10 Å^{-1}, Rh–O phase shift corrected) [solid line = |FT'|, dotted line = ImFT'].

I. $Rh(CO)_2$ Reference Compound. The EXAFS signal of the rhodium K-edge of a physical mixture of $\{Rh(CO)_2Cl\}_2$ and silica was recorded at liquid nitrogen temperature in a CO atmosphere (10^2 kPa) (see Figure 6a). As can be seen from the structure of the dimer (Figure 5) the EXAFS is mainly caused by three scatterer pairs: Rh–Cl, Rh–C, and Rh–O* (oxygen of the carbonyl). Figure 6b shows the imaginary part (dotted line) and the absolute value (solid line) of the associated k^2-weighed Fourier transform, through which the best splitting of the separate neighbor shells in r space was obtained. The Fourier transform was performed on a k interval from 2.44 to 12.6 Å^{-1} and corrected for Rh–O phase shift. The corrected Fourier transform is denoted by FT′. The phase shift correction deserves some closer attention. In general, a phase shift correction on the Fourier transform is applied in order to obtain real interatomic distances R in r space as well to obtain symmetrical functions of the imaginary part ImFT′ and the absolute value |FT′|.[30] By using an Rh–O phase shift correction the Rh–O as well as the Rh–C and the Rh–Cl coordinations peak at real interatomic distances in FT′ because (a) the scatterer behavior of an Rh–C and Rh–O scatterer pair hardly differ and (b) the difference between the Rh–O and the Rh–Cl phases is nearly π, which means that the imaginary part of the Rh–O phase-shift-corrected radial distribution function of the Rh–Cl EXAFS peaks negatively, but nearly at the exact real interatomic Rh–Cl distance. The contribution of each of the three scatterer pairs to the FT′ is to be found then at their corresponding real interatomic distances. Therefore, the three peaks in the radial distribution function (Figure 6b) are assigned to the following: Rh–C, Rh–Cl, and Rh–O* at R = 1.8, 2.4, and 2.9 Å, respectively. Note that the imaginary part of the Rh–Cl contribution peaks negatively around 2.4 Å. To obtain a proper reference EXAFS signal for $Rh(CO)_2$ the contribution of Rh–Cl has to be subtracted from the rhodium EXAFS of the dimer. This was carried out by calculating the Rh–Cl EXAFS with the known crystallographic parameters and subtracting it from the primary EXAFS data. The phase shift and backscattering amplitude were obtained from EXAFS measurements on $RhCl_3$. The criterion used for a proper determination of the Rh–Cl parameters was a decrease of the amplitude of the Rh–Cl peak in the |FT′| of the $\{Rh(CO)_2Cl\}_2$ complex to the noise level. The parameter values thus obtained for the Rh–Cl bond in the rhodium complex were the following: R = 2.36 Å (from X-ray diffraction R = 2.355 Å), N(Rh–Cl) = 2.1, and $\Delta\sigma^2$ = 0.001 Å^2 (relative to $RhCl_3$).

Figure 6c shows the $Rh(CO)_2$ EXAFS signal obtained by subtracting the calculated Rh–Cl contribution from the primary EXAFS function. The k^2-weighed (Rh–O phase shift corrected) Fourier transform of the residual EXAFS signal is given in Figure 6d. The oxygens of the carbonyl ligands are clearly visible. As the carbon atom lies between the absorber, rhodium, and the scatterer, oxygen, one must take into account depletion of the primary outgoing wave as well as phase changes caused by the intervening atom. Although one might intuitively expect atoms directly behind the first set of scatterers to have little contribution to the EXAFS, the opposite is actually true. The amplitude is much more pronounced than one would have expected on the basis of the simple N/R^2 dependence of the amplitude. Apart from this amplitude anomaly the Rh–O* peak shows a phase shift of π radians, as is clear from the fact that the imaginary part peaks negatively at R = 3.00 Å. Similar deviations of the amplitude and anomalous phase shifts have been observed previously in the Fourier transform spectra of $Mo(CO)_6$[31] and $Na_2Fe(CO)_4$,[32] and they have been interpreted as the result of multiple scattering processes.

The Rh–C and Rh–O* distance were determined by a phase analysis of the representative Fourier-filtered signals. As no Rh–C reference compound was available, we used the theoretical phase given by Teo and Lee[33] in order to determine the Rh–C distance.

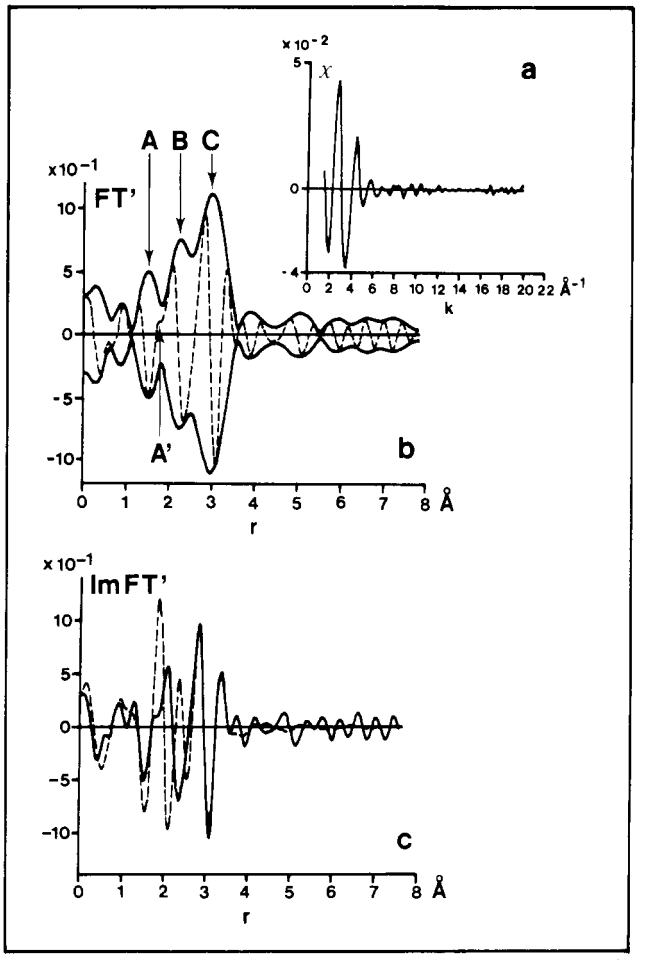

Figure 7. Rh (0.57 wt %)/γ-Al_2O_3 after CO admission at 298 K; (a) the normalized smoothed EXAFS data of the rhodium K-edge at 77 K; (b) the associated k^3-weighed Fourier transform (Δk = 3.24–8.4 Å^{-1}, Rh–O phase shift corrected) [solid line = |FT′|, dotted line = ImFT′]; (c) the imaginary parts of the k^3-weighed Fourier transforms of the normalized smoothed EXAFS data (solid line) and the calculated contribution of Rh–C–O* fine structure (dotted line) (Δk = 3.24–8.4 Å^{-1}, Rh–O phase shift corrected).

For the determination of the Rh–O* distance we used the reference Rh–O phase which was adjusted with a factor π for reasons mentioned above. The obtained bond lengths of Rh–C and Rh–O* are 1.85 and 3.00 Å, respectively, and are in good agreement with the values determined by X-ray diffraction (cf. Figure 5).

The backscattering amplitude and phase obtained by inverse transformation (Δr = 1.25–3.47 Å) of the radial distribution function as presented in Figure 6d can now be used as reference for $Rh(CO)_2$ in the subsequent analysis of the EXAFS spectrum of the catalyst after CO adsorption.

II. 0.57 wt % Rh/Al_2O_3 + CO. It is clear that the smoothed EXAFS functions of the catalyst after CO adsorption at room temperature (Figure 7a) and the $Rh(CO)_2$ reference compound (Figure 6c) differ significantly. This indicates that the EXAFS of the catalyst is not caused by Rh–C and Rh–O* coordination only. Another Rh–Z scatterer contribution might originate from the elements through which the geminal dicarbonyl is anchored to the support. The element can be oxygen and/or chlorine, anions of which are still present after reduction of the catalyst, as observed by XPS.

Figure 7b shows the k^3-weighed and Rh–O phase-shift-corrected Fourier transform of the smoothed EXAFS data, performed on a k interval from 3.24 to 8.4 Å^{-1}. A good splitting of the separate neighbor shells in r space was obtained, and within the r interval of 1–3 Å three peaks could be distinghuished: peak A at 1.8 Å and peak C at 3.0 Å were assigned to respectively Rh–C and Rh–O*, both originating from $Rh(CO)_2$ species, whereas peak B at 2.4 Å is a contribution of the as yet unknown Rh–low-Z

(30) Lee, P. A.; Beni, G. *Phys. Rev. B* **1975**, *11*, 1279.
(31) Cramer, S. P.; Hodgson, K. O.; Stiefel, E. I.; Newton, W. E. *J. Am. Chem. Soc.* **1978**, *100*, 2748.
(32) Teo, B. *J. Am. Chem. Soc.* **1981**, *103*, 3990.
(33) Teo, B.; Lee, P. A. *J. Am. Chem. Soc.* **1979**, *101*, 2815.

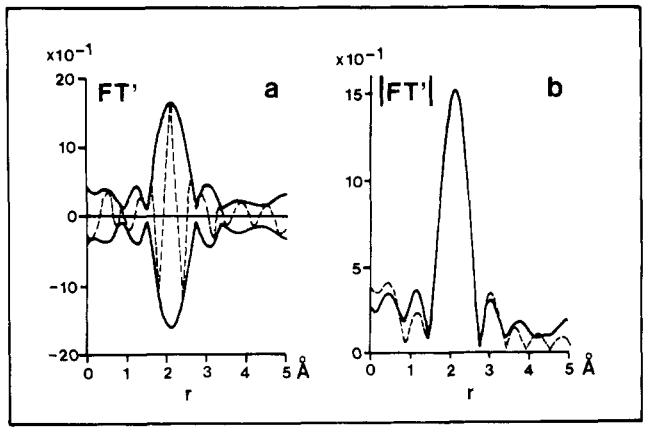

Figure 8. Rh (0.57 wt %)/γ-Al_2O_3 after CO admission at 298 K: (a) the k^3-weighed Fourier transform of the difference signal between the normalized smoothed EXAFS data and the calculated contribution of Rh–C–O* fine structure (Δk = 3.3–8.4 Å^{-1}, Rh–O phase shift corrected); (b) the k^3-weighed Fourier transforms of the difference signal (solid line) and the calculated fine structure of nearest neighbor oxygen atoms (dotted line) (Δk = 3.3–8.4 Å^{-1}, Rh–O phase shift corrected).

element pair. From the imaginary part (Figure 7b) it can be seen that the Rh–C signal is suppressed to a great extent at position A′, whereas the Rh–O* signal around 3.0 Å has hardly been affected by interference with peak B. By matching the imaginary part above r = 2.6 Å with ImFT′ of a calculated $Rh(CO)_2$ EXAFS, using the phase and amplitude of the geminal dicarbonyl reference compound, we obtained the contribution of $Rh(CO)_2$ oscillations to the EXAFS of the catalyst. This is illustrated in Figure 7c. The optimized parameter values are N(Rh–(CO)) = 1.8 and $\Delta\sigma^2$ = 0.007 Å^2 relative to $\{Rh(CO)_2Cl\}_2$, both for Rh–C and Rh–O*. The interatomic distances were kept equal to the Rh–C–O* distances in the dimer. The average coordination is, within the limits of accuracy, in good agreement with the CO chemisorption result (CO/Rh = 1.9) and again demonstrates that $Rh(CO)_2$ species were formed.

In order to determine the type of scatterer responsible for peak B, the difference signal between the smoothed EXAFS data and the calculated EXAFS of $Rh(CO)_2$ has been analyzed. The imaginary part and the absolute value of the k^3-weighed Fourier transform corrected for Rh–O phase shift of the difference signal are given in Figure 8a. Note that the imaginary part is symmetrical and peaks positively and that the maximum coincides with the peak maximum of the absolute value. Consequently, this contribution to the spectrum is caused by Rh–O coordination. Table III presents the optimized parameter values, obtained by fitting the EXAFS in k space, by which the difference signal is described best. The absolute values of the radial distribution functions of the calculated one-shell Rh–O EXAFS, using the optimized parameters, and the difference signal are given in Figure 8b. The average coordination number for the Rh–O distance is 3.1, which indicates that the geminal dicarbonyl is anchored to the support by three oxygen ions with equal interatomic distances of 2.12 Å. The bond length of 2.12 Å indicates that rhodium is in an oxidic state. The distance is 0.07 Å longer than the first shell distance of Rh–O in Rh_2O_3, which implies that the average oxidation state of rhodium is lower than 3+.

As a final check we calculated an EXAFS function including Rh-support oxygen, Rh–C, and Rh–O* bonds in $Rh(CO)_2$, using the optimized parameter values (cf. Table III). The calculated EXAFS shows excellent agreement with the EXAFS data (Figure 9a). The imaginary parts and the absolute values of the associated Fourier transforms match very well, as can be seen in Figure 9b and Figure 9c, respectively.

ESR. If the oxidation state of the observed isolated $Rh(CO)_2$ species were zero, it should be possible to detect an ESR signal of Rh^0 after CO admission, since Rh^0 (d^8s^1) is paramagnetic. Reduction and evacuation of the catalyst at 593 K and subsequent admission of CO, followed by an evacuation at room temperature, gave rise to the ESR spectrum presented in Figure 2b, which is

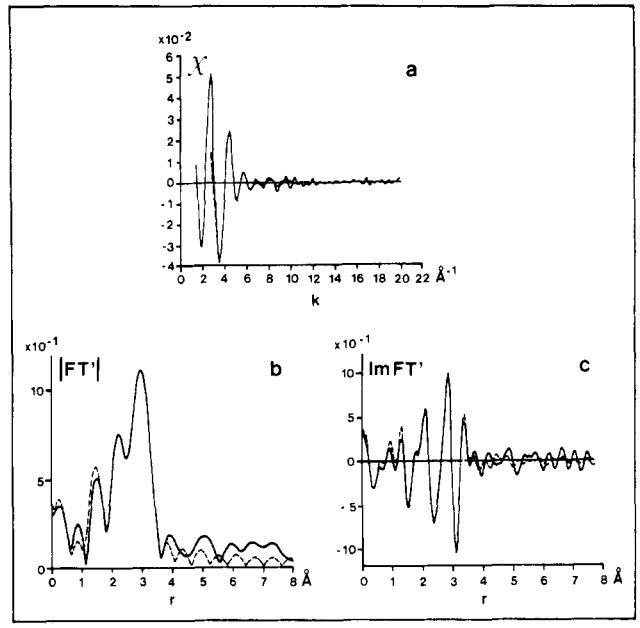

Figure 9. Rh (0.57 wt %)/γ-Al_2O_3 after CO admission at 298 K. The solid lines represent the data and the dotted lines represent the calculated two-shell fit (Rh–C–O*, Rh–O) with the optimized parameter values (cf. Table III): (a) $\chi(k)$ of the rhodium K-edge vs. k; (b) the associated |FT′|; and (c) the associated ImFT′, k^3-weighed FT′ (Δk = 3.24–8.4 Å^{-1}, Rh–O phase shift corrected).

completely different from the spectrum obtained after reduction. The total ESR intensity is very low, which indicates that the majority of the rhodium present, that is the $Rh(CO)_2$ species, is not paramagnetic. Therefore, the oxidation state of rhodium in $Rh(CO)_2$ cannot be zero, (nor 2+) and must either be 1+ or 3+.

The ESR spectrum consists of two separate signals. Firstly, a signal with g = 2.09 (ΔH = 250 G) and a shoulder at g = 2.26, and secondly, a signal with $g_\parallel$ = 2.043 and $g_\perp$ = 2.011 ($\Delta H_\perp$ = 26 G). We assign the first ESR signal to Rh^{2+}. The difference with the signal observed after reduction indicates that a change in the environment of the Rh^{2+} ions has taken place, probably due to alteration in the electronic properties of the metal ion caused by for instance back donation of electrons from Rh to CO. The line width of the second signal is remarkably small (26 G), and no hyperfine splitting due to the rhodium nucleus is observed. This suggests that this signal belongs to a radical which has only a small spin density on a rhodium atom or ion. It might be due to an oxygen or CO radical. The CO chemisorption measurements showed that the bare support Al_2O_3 adsorbed a considerable amount of CO molecules, a small part of which might become paramagnetic when in contact with Rh, because adsorption of CO on pure Al_2O_3 did not give an ESR signal. With thermally activated MgO and ThO_2, formation of radicals upon adsorption of CO at 298 K had indeed been reported.[34]

XPS. In order to obtain more information about the oxidation state of the rhodium after CO admission we compared the rhodium $3d_{5/2}$ electron binding energies of the catalyst and the $\{Rh(CO)_2Cl\}_2$ exchanged alumina in which the valence of rhodium is 1+. The results are presented in Table II, and they clearly show that within the experimental error both binding energies are equal (308.6 ± 0.1 eV). This indicates that the oxidation state of rhodium after CO admission is 1+. Thus, the oxidation state of rhodium in the highly dispersed catalyst changes from zero, after reduction, to 1+ when CO is admitted, and consequently, CO adsorption has to be accompanied by an oxidation process for ultradispersed rhodium supported on alumina.

Discussion

The Structure of Rhodium after Reduction. The TPR results show that the degree of reduction of the reduced catalyst was high

(34) Cordischi, D.; Indovina, V.; Occhiuzzi, M. *J. Chem. Soc., Faraday Trans. 1* **1980**, *76*, 1147.

(95 ± 5%). We therefore exclude the possibility of rhodium being completely or to a great extent dispersed as isolated Rh^{1+} ions. Since an Rh^0 (d^8s^1) ESR signal could not be detected, no isolated rhodium atoms are present either. We thus conclude that only rhodium metal crystallites exist in the highly dispersed Rh/γ-Al_2O_3 catalyst after reduction with hydrogen, as is indeed proved by the EXAFS results and as was previously concluded from results obtained with other techniques.[7,8,35]

The low average coordination number of 3.7 (Table III) indicates that the crystallites are very small. As might have been expected, a substantial contribution of rhodium–carrier oxygen EXAFS oscillations is observed.[28] The Rh–O interatomic distance of 2.74 Å (2.05 Å in Rh_2O_3) indicates that the interaction between the particle and the support occurs via Rh atoms and oxygen ions of the alumina, and not via interdiffusion of the metal oxide and the oxidic support as proposed by Anderson[36] and well established for systems such as Ni/SiO_2, Ni/Al_2O_3, and Co/Al_2O_3.[37-39]

On the basis of the present EXAFS results we cannot distinguish between two-dimensional and three-dimensional rhodium crystallites. However, EXAFS measurements carried out on another ultradispersed Rh (0.47 wt %)/γ-Al_2O_3 catalyst, reduced at 773 K but with a high H/Rh value of 1.7, resulted in an average coordination number of the Rh–Rh and Rh–O distance of 5.3 and 1.3, respectively.[40] In this catalyst the rhodium metal particles are somewhat larger, compared to the crystallites of the catalyst reduced at 593 K, but are still very small as indicated by the observed relatively low coordination number of the Rh–Rh distance and the high H/Rh value. It is obvious that the structure of the particles in both catalysts is similar. If we are dealing with a two-dimensional structure one expects that the average coordination number of the Rh–O distance is constant and independent of the size of the raft. However, going from a particle with N(Rh–Rh) = 3.7 to a particle with N(Rh–Rh) = 5.3 the N-(Rh–O) changes from 1.9 to 1.3. Therefore, we think that the most likely structure of the metal particles is three dimensional. This conclusion is not in accordance with the conclusion reached by Yates et al. on the basis of TEM measurements.[10,11] However, TEM is an ex situ technique. In order to prepare a sample specimen the sample must be handled in air. Consequently, the catalyst studied in the TEM investigation will have been passivated. The TPR results show that a passivated highly dispersed rhodium catalyst will be almost completely oxidized. This then explains the TEM results, because it is known that several transition-metal oxides, including rhodium oxide which is stable at room temperature at an oxygen pressure above 2×10^{-19} Pa, may form a well-dispersed two-dimensional phase, the so-called δ phase, on alumina.[41]

Although the rhodium particles are very small and consequently the greater part of the rhodium atom is exposed, the interatomic distance between the rhodium atoms is similar to the distance in Rh foil (Table III). Many LEED studies have reported differences between the interplanar spacings of the surface layers of single crystals and bulk spacings. An example is the work on Ni (110) for which a 5% contraction has been found.[42] Therefore, one would also expect a contraction of the Rh–Rh bond in the small particles. However, during the present EXAFS measurements the rhodium was covered with hydrogen. Therefore, the rhodium surface atoms were coordinatively saturated, thus relaxing the Rh–Rh bonds. For single-crystal surfaces it has been observed

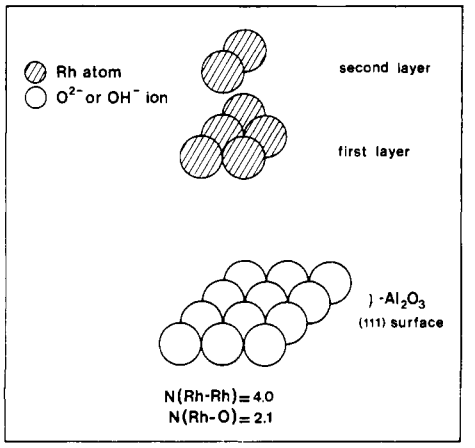

Figure 10. Possible structure of rhodium crystallites with an fcc structure in the 0.57 wt % Rh/γ-Al_2O_3 catalyst reduced at 593 K.

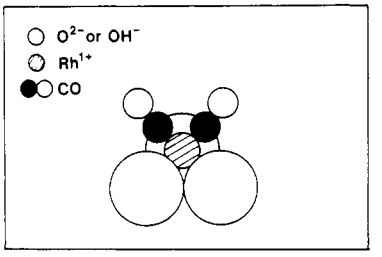

Figure 11. Possible structure of $Rh(CO)_2$ species attached to the γ-Al_2O_3 support after CO admission at 298 K.

that when a surface is covered by an adsorbed layer, the top substrate layer relaxes.[43] Moraweck et al.[44] have observed with EXAFS a contraction of the Pt–Pt distance in a Pt/Y–zeolite sample of 0.12 Å when the particles were measured in an He environment. A subsequent H_2 admission at room temperature relaxed the bond to a distance similar to that in Pt foil. Very recently[45] we have conducted EXAFS measurements after purging with helium and indeed observed a contraction of the Rh–Rh distance.

At the end of this part of the discussion we want to propose a possible structure of the rhodium crystallites formed during reduction of the catalyst under investigation. According to Knözinger and Ratnasamy[46] the surface of γ-Al_2O_3 consists of different types of planes (e.g. (111), (110), and (100)). A possible structure for a rhodium crystallite, with an fcc structure and Rh–Rh and Rh–O coordination numbers which approach the experimental ones (4.0 and 2.1 vs. 3.7 and 1.9), on a (111) plane is presented in Figure 10.

The Structure of Rhodium after CO Admission. The EXAFS results clearly show the dramatic influence of CO chemisorption on the structure of small Rh particles in the ultradispersed 0.57 wt % Rh/γ-Al_2O_3 catalyst. The metallic crystallites, formed during reduction, break up to rhodium geminal dicarbonyl species during CO admission, as proven by infrared and EXAFS. The geminal dicarbonyl species have support oxygen anions as ligands, as established by the analysis of the EXAFS spectrum of the CO adsorbed catalyst. The quantitative results demonstrate that rhodium is surrounded by two CO molecules and three oxygen anions of the support. The $Rh(CO)_2$ species can be attached to the (111) surface of the γ-Al_2O_3 via 3 oxygen atoms as presented in Figure 11.

There are two possible ways for explaining why no Rh–Rh distances are observed in the EXAFS after CO adsorption: either the Rh–Rh distances in the resulting aggregate of $Rh(CO)_2$ species

(35) Katzer, J. R.; Sleight, A. W.; Gajardo, P.; Michel, J. B.; Gleason, E. F.; McMillan, S. *Farada Discuss.* **1981**, *72*, 121.
(36) Anderson, J. R. "The Structure of Metallic Catalysts"; Academic Press: London, 1975.
(37) Derouane, E. G.; Simoens, A. J.; Vedrine, J. C. *Chem. Phys. Lett.* **1977**, *52*, 549.
(38) Shalvoy, R. B.; Davis, B. H.; Reucroft, P. J. *Surf. Int. Anal.* **1980**, *2*, 11.
(39) Greegor, R. B.; Lytle, F. W.; Chin, R. L.; Hercules, D. M. *J. Phys. Chem.* **1981**, *85*, 1232.
(40) van 't Blik, H. F. J.; van Zon, J. B. A. D.; Koningsberger, D. C.; Prins, R. *J. Mol. Catal.* **1984**, *25*, 379.
(41) Yao, H. C.; Shelef, M. *J. Catal.* **1976**, *44*, 392.
(42) Demuth, J. E.; Marcus, P. M.; Jepsen, D. W. *Phys. Rev. B* **1975**, *11*, 1460.
(43) Marcus, P. M.; Demuth, J. E.; Jepsen, D. W. *Surf. Sci.* **1975**, *53*, 501.
(44) Moraweck, B.; Clugnet, G.; Renouprez, A. J. *Surf. Sci.* **1979**, *81*, L631.
(45) van Zon, J. B. A. D.; Koningsberger, D. C., to be published.
(46) Knözinger, H.; Ratnasamy, R. *Catal. Rev.-Sci. Eng.* **1978**, *17*, 31.

have increased somewhat and have a too large spread to see any EXAFS oscillations at higher k value or the $Rh(CO)_2$ species are indeed rather far apart on the support. In view of the mild conditions under which the particles have been treated we prefer the former explanation in which the small metal clusters expand under the influence of CO. This hypothesis has been proposed earlier by Yates et al.,[11] who called the phenomenon a "breathing raft". Measurements performed on another highly dispersed rhodium catalyst[40] showed that the aggregate of $Rh(CO)_2$ species rearranged after desorption of CO at elevated temperatures to metallic particles. Thus, the process of disruption of the metal particles by CO is reversible and these particles can indeed be called "breathing rafts or particles".

From the fact that no paramagnetic ESR Rh^0 (d^8s^1) signal could be detected after CO admission and from the Rh–O distance determined by EXAFS, we infer that CO adsorption has to be oxidative. The oxidation state of rhodium in the $Rh(CO)_2$ species is most likely 1+, as confirmed by XPS and IR and as suggested originally by Primet[7] and in our short communication.[10] In view of the observed reaction[47,48] between surface OH groups and $Rh_6(CO)_{16}$, the most likely explanation for the oxidation to Rh^{1+} is that hydroxyl groups react with rhodium carbonyl species:

$$6Rh^0 + 6nCO \rightarrow 6Rh(CO)_n$$

$$6Rh(CO)_n + (16 - 6n)CO \rightarrow Rh_6(CO)_{16}$$

$$Rh_6(CO)_{16} + 6Al\text{–}OH \rightarrow 3H_2 + 6Al\text{–}O\text{–}Rh(CO)_2 + 4CO$$

A gas chromatographic analysis of the gas over the catalyst after CO chemisorption did not supply evidence for H_2 formation, however. Although the detection system may have been too insensitive, this may indicate that rhodium is oxidized by a dissociatively adsorbed CO molecule:

$$CO + 3Rh \rightarrow RhC + 2Rh^{1+} + O^{2-}$$

$$2Rh^{1+} + 4CO \rightarrow 2Rh^{1+}(CO)_2$$

Although adsorption of CO on large Rh particles is not dissociative at room temperature,[49,50] this is probably not the case when the particle size decreases below 10 Å. For these reasons we suggest that the oxidation of the rhodium atoms might be coupled to the dissociation of CO. In that case the reverse reaction (we observed that metal particles are reformed when evacuating at 573 K) might take place as a reductive desorption of CO according to the reaction

$$O^{2-} + 2Rh^{1+}(CO)_2 \rightarrow 2Rh + CO_2 + 3CO$$

Conclusions

From the results of this study performed on a highly dispersed 0.57 wt % $Rh/\gamma\text{-}Al_2O_3$ catalyst two main conclusions can be drawn. In the first place after reduction at 593 K the catalyst is highly dispersed. Only small metal crystallites are present consisting of 6–10 atoms and probably they have a three-dimensional structure. No indications for the existence of dispersed rhodium atoms or ions after reduction have been observed. The metal–support interactions involve Rh^0–(carrier)O^{2-} bonds. All this demonstrates that there is no fundamental difference between reduced Rh/Al_2O_3 catalysts with low Rh loading and those with high Rh loading. At all loadings rhodium metal crystallites are present on the support surface. Only the size and morphology of these crystallites vary with Rh loading.

The second conclusion of our study is that adsorption of CO at room temperature on the 0.5 wt % $Rh/\gamma\text{-}Al_2O_3$ catalyst results in a significant disruption of the Rh crystallites, ultimately leading to isolated rhodium geminal dicarbonyl species in which rhodium has an oxidation state of 1+ and is surrounded by two carbon monoxide molecules and three oxygen ions. The adsorption of CO is oxidative and can be explained by dissociation of CO followed by CO adsorption on the oxidized rhodium.

The results of this study explain the apparent contradiction between the results obtained from infrared studies and those obtained from high-resolution electron microscopy. This contradiction is, indeed, apparent because as our EXAFS measurements prove, CO adsorption changes the system completely. After reduction and before CO admission small Rh metal crystallites are present, whereas after CO admission isolated $Rh(CO)_2$ species are on the support. The large difference in structure between an Rh catalyst before and after adsorption of CO might not be an isolated case but might be an example of a more general phenomenon of a drastic change in catalyst structure upon adsorption of an adsorbate. Such cases might especially be expected for adsorbates which are adsorbed with large heats of adsorption on small catalyst crystallites.

The present study beautifully shows the strength of the EXAFS technique. If only one type of species is present, as was the case here for the $Rh^{1+}(CO)_2$ species, and if a careful analysis is made of sample and reference samples, detailed structural information can be obtained. In fact, the only point left to be studied about the geminal dicarbonyl rhodium species is if it would be possible, with much improved signal to noise, to see something of the distance between such species. On the other hand, even though the average number of rhodium and oxygen neighbors of the rhodium atoms in the very small rhodium crystallites in the reduced catalyst is known, still no unambiguous choice can be made on the basis of the results of one catalyst alone if these crystallites have a two- or a three-dimensional shape. Better data, probably to be obtained with fluorescence detection, might provide information on higher coordination shells and might allow a distinction to be made between the shape models for each catalyst.

Acknowledgment. The EXAFS part of this study was done at SSRL (Stanford University), which is supported by the NSF through the Division of Materials Research and the NIH through the Biotechnology Resource Program in the Division of Research Resources in cooperation with the Department of Energy. We gratefully acknowledge the assistance of the SSRL staff and thank Dr. D. E. Sayers for fruitful discussions. This study was supported by the Netherlands Foundation for Chemical Research (SON) with financial aid from the Netherlands Organization for the Advancement of Pure Research (ZWO). One of us (D.C.K.) thanks ZWO for supplying a travel grant (R71-34).

(47) Smith, A. K.; Hugues, F.; Theolier, A.; Basset, J. M.; Ugo, R.; Zanderighi, G. M.; Bilhou, J. L.; Bilhou-Bougnot, V.; Graydon, W. F. *Inorg. Chem.* **1979**, *18*, 3104.

(48) Theolier, A.; Smith, A. K.; Leconte, M.; Basset, J. M.; Zanderighi, G. M.; Psaro, R.; Ugo, R. *J. Organomet. Chem.* **1980**, *191*, 415.

(49) Yates, J. T., Jr.; Williams, E. D.; Weinberg, W. H. *Surf. Sci.* **1981**, *91*, 562.

(50) Castner, D. G.; Dubois, L. H.; Sexton, B. A.; Somorjai, G. A. *Surf. Sci.* **1981**, *103*, L 134.